NONLINEAR MICROMECHANICS OF FAILURE FOR STRENGTH PREDICTION OF COMPOSITE LAMINATES

Y. C. Huang, K. K. Jin, S. K. Ha
Department of Mechanical Engineering, Hanyang University
#1271, Sa 1-dong, Sangnok-gu, Ansan-si, Gyeonggi-do, 426-791, Republic of Korea
sungha@hanyang.ac.kr

SUMMARY

Nonlinear micromechanics of failure (MMF), which combines independent constituent failure criteria and progressive damage model, was developed to predict the constitutive behavior and strength of composite laminates under multi-axial loadings. Good agreement between theoretical prediction and test data was achieved.

Keywords: micromechanics, nonlinear, strength, constituent, failure criterion, progressive damage, multi-axial loading

INTRODUCTION

During the past half century, a great deal of research has been dedicated to investigating failure mechanism of composite materials. New failure theories have kept emerging in this field, some of which have been widely accepted and employed in industries to guide the design of composite structures. Today a rapid growth of composite applications in various industries requires new failure prediction of composite materials with the capability of dealing with multi-axial combined loadings, catching the nonlinear constitutive behavior, predicting initial and final failure of a laminate, and etc. Recently, a new failure theory called micromechanics of failure (MMF), based on unit cell model which describes microstructure of composite and independent failure criterion for each constituent, was proposed in order to meet the new challenges mentioned above [1]. The three-dimensional unit cell model guarantees MMF is naturally capable of dealing with problems involving fully three-dimensional multi-axial loadings; while the constituent failure criteria make it possible to distinguish the critical constituent/constituents in the critical ply/plies. However, the constitutive behavior of both fiber and matrix was assumed to be linear elastic at the first stage, which made it impossible to predict the considerably nonlinear behavior of a unidirectional laminate subject to transverse tension/compression or in-plane shear, as revealed by a large number of experiments. Therefore, the MMF theory was incorporated with a progressive damage model for the polymeric matrix, which is the major contributor of nonlinearity.

MICROMECHANICS OF FAILURE AND PROGRESSIVE DAMAGE MODEL

Micro Stress and Macro Stress

In order to express micro structure of one lamina in terms of fiber, matrix, and interface, a unit cell model was devised (Fig. 1). With this model, constituent behavior is directly related to ply behavior. Usually, carbon fiber is taken as transversely isotropic, while glass fiber as isotropic. We accepted this assumption, and further assumed both carbon and glass fibers to be linear elastic and brittle. On the other hand, the polymeric matrix was assumed to be isotropic and ductile, featuring nonlinear behavior once it is damaged. The fiber-matrix interface was modeled to exhibit linear traction-separation behavior.

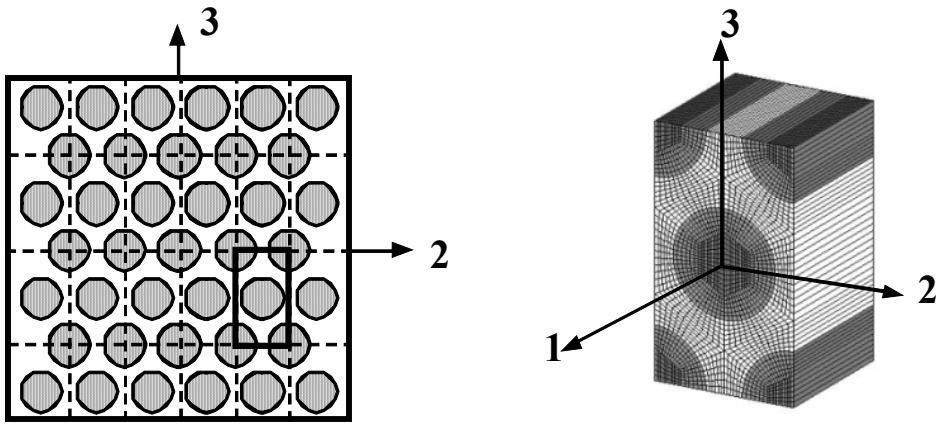

Fig. 1. Unit cell model (hexagonal fiber array).

Though the UD ply is generally considered to be transversely isotropic, the strain/stress distribution within fiber and matrix, as well as the interfacial traction distribution along the fiber-matrix interface, must be non-uniform even under uniform external loading conditions due to the inhomogeneity at micro level. The distribution of micro stresses was related to macro stresses and temperature increment as [2]:

$$\begin{aligned} \boldsymbol{\sigma}_f &= \mathbf{M}_f \bar{\boldsymbol{\sigma}} + \mathbf{A}_f \Delta T \\ \boldsymbol{\sigma}_m &= \mathbf{M}_m \bar{\boldsymbol{\sigma}} + \mathbf{A}_m \Delta T \\ \mathbf{t} &= \mathbf{M}_i \bar{\boldsymbol{\sigma}} + \mathbf{A}_i \Delta T \end{aligned} \tag{1}$$

where $\bar{\boldsymbol{\sigma}}$, $\boldsymbol{\sigma}_f$, $\boldsymbol{\sigma}_m$, and $\mathbf{t}_i$ represent macro stresses, micro stresses in fiber, micro stresses in matrix, and interfacial tractions, respectively. Stress amplification factors for macro stress **M** and for temperature increment **A** were determined through direct finite element analysis of a unit cell with proper boundary conditions.

Constituent Failure Criteria and Progressive Damage Model

A complete set of constituent failure criteria were proposed [3]. A maximum longitudinal stress failure criterion was used for the fiber:

$$-C_f < \sigma_{f11} < T_f \tag{2}$$

where σ_{f11} denote the micro fiber longitudinal stress, while T_f and C_f denote fiber longitudinal tensile and compressive strength, respectively. Matrix materials are, in most cases, isotropic, but have different tensile and compressive strengths. Numerous experiments have shown that crazing or failure in matrix is more sensitive to tensile stresses than compressive stresses. Such different tensile and compressive strengths indicate that matrix failure depends not only on the deviatoric stress invariant, i.e. von Mises equivalent stress σ_{VM}, but also on the volumetric stress invariant, i.e. the first stress invariant I_1. Raghava *et al.* suggested a modified version of the von Mises failure criterion [4] in terms of initial tensile strength T_{mi} and compressive strength C_{mi} :

$$\frac{\sigma_{VM}^2}{C_{mi}T_{mi}}+\left(\frac{1}{T_{mi}}-\frac{1}{C_{mi}}\right)I_1=1 \tag{3}$$

This failure criterion is equivalent to the condition that an equivalent stress σ_{eq} reaches the initial tensile strength T_{mi} :

$$\sigma_{eq}=\frac{(\beta-1)I_1+\sqrt{(\beta-1)^2 I_1^2+4\beta\sigma_{VM}^2}}{2\beta} \tag{4}$$

where β is defined as the ratio of matrix initial compressive to initial tensile strengths. The equivalent stress σ_{eq} is often called the Stassi's stress. We adopted Eq. (3) as the initial failure criterion for the matrix.

Once failure occurs, damage starts to develop and the stiffness of matrix reduces according to the amount of damage accumulated inside the matrix. We took the damage initiation and propagation as isotropic, and the constitutive relation of the matrix was given as:

$$\boldsymbol{\sigma}_m=(1-D_m)\mathbf{C}_m\boldsymbol{\varepsilon}_m \tag{5}$$

where the damage factor D_m must be in the range between 0 and 1. After initiation of failure, the relation between the equivalent stress σ_{eq} and damage factor D_m was described by the following equation:

$$D_m=1-\exp\left[\gamma(1-k_m)\right] \tag{6}$$

where k_m is the matrix failure index, defined as the ratio of σ_{eq} to T_{mi} , γ being a parameter used to calibrate the uniaxial stress-strain curves based on test data. Furthermore, the constitutive relation was complemented by a damage loading function:

$$f\left(\sigma_{eq},\kappa\right)=\sigma_{eq}-\kappa_m \tag{7}$$

where κ_m is a scalar-valued history variable starting at a threshold level T_{mi} at which damage is initiated and is updated as required by the Kuhn-Tucker loading-unload condition:

$$f\le 0,\ \dot{\kappa}_m\ge 0,\ f\dot{\kappa}_m=0 \tag{8}$$

The final fracture usually occurs before the damage factor D_m attains to the unity. This value can be determined from the uniaxial tensile stress-strain curve. A value of

0.4 was used as a practical value for the rupture criterion of a damaged material [5]. As for the interface, although we proposed a quadratic failure criterion for it, in this article we simply assumed the bonding between fiber and matrix is strong enough not to produce any separation at the interface. This is often true if proper surface treatment for fiber is executed in order to enhance interfacial strength, just as many manufacturers do.

The overall scenario which combines MMF and progressive damage model is shown in Fig. 2. At the beginning of one global time increment *i*, first calculate the total macro strain $\overline{\boldsymbol{\varepsilon}}^{(i)}$ after current time increment, which is the summation of total macro strain before current time increment $\overline{\boldsymbol{\varepsilon}}^{(i-1)}$, and the macro strain increment $\Delta\overline{\boldsymbol{\varepsilon}}^{(i)}$, then calculate the macro stress $\overline{\boldsymbol{\sigma}}^{(i)}$ based on previous effective ply stiffness $\overline{\mathbf{C}}^{(i-1)}$ and $\overline{\boldsymbol{\varepsilon}}^{(i)}$. Next compute micro stress in fiber $\overline{\boldsymbol{\sigma}}_f^{(i)}$ and in matrix $\overline{\boldsymbol{\sigma}}_m^{(i)}$ due to macro stress and temperature increment. The following procedures involve applying constituent failure criteria to fiber and matrix, getting their respective failure indices, employing progressive damage model to get degraded fiber and matrix moduli, and calculating effective ply stiffness through micromechanical model for next global time increment. The calculation was performed with commercial FEA software MD Nastran combined with user-defined subroutine UFAIL and UPROGFAIL [6], as well as Abaqus 6.7-1 combined with user-defined subroutine UMAT [7].

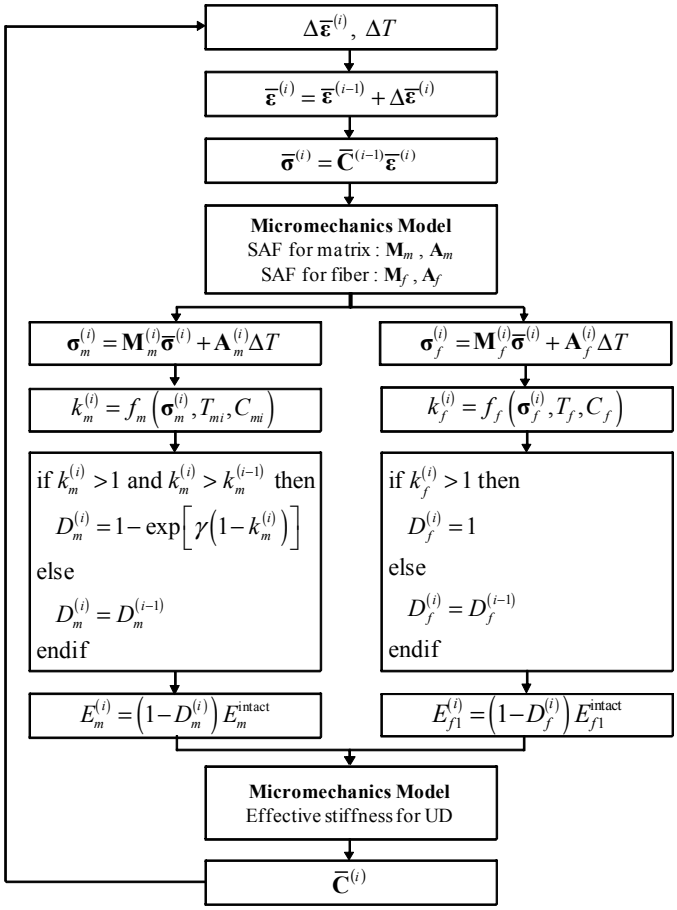

Fig. 2. Overall algorithm combining the MMF and progressive damage model.

Variation of Ply Moduli and Stress Amplification Factors with Constituent Moduli

As the damage of matrix evolves, the Young's modulus of matrix decreases accordingly, resulting in the reduction of ply moduli. Usually, the Young's modulus of fiber in its longitudinal direction is much higher than that of matrix, therefore based on our assumption that fiber is linear elastic and brittle, the damage of matrix has little influence on the Young's modulus of ply in its longitudinal direction. This can be easily verified by employing simple rule of mixture for a reasonable fiber volume fraction V_f. Nevertheless, other ply moduli show remarkable dependence on both fiber and matrix moduli. Fig. 3(a) and (b) show variation of ply transverse modulus and shear moduli with respect to their constituent counterparts, respectively. In Fig. 3, matrix Young's modulus E_m and shear modulus G_m range from 0 to 10 GPa, while fiber transverse Young's modulus E_{f22} , in-plane shear modulus G_{f12} , and out-of-plane shear modulus G_{f23} range from 0 to 100 GPa. We also assumed that V_f=0.6, ν_m = 0.35, ν_{f12} = ν_{f23} = 0.2. The dependency of ply in-plane shear modulus $\overline{G}_{12}$ on G_{f12} and G_m is almost identical with that of ply out-of-plane shear modulus $\overline{G}_{23}$ on G_{f23} and G_m , so they were plotted together. Judging by the shape of two surfaces, we concluded that the dependencies shown in two subplots are quite similar.

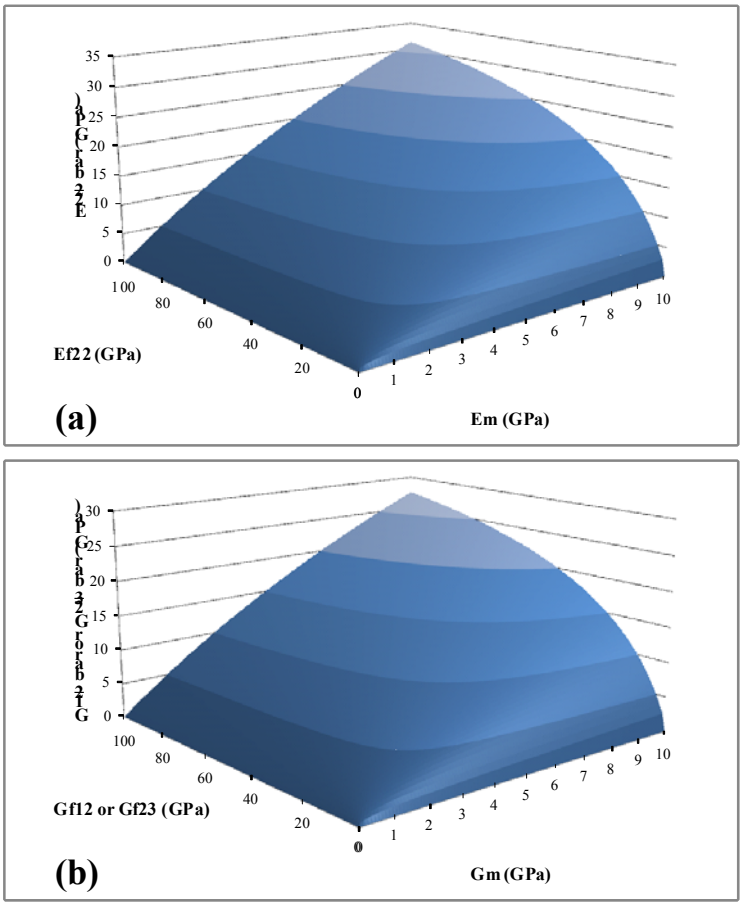

Fig. 3. Variation of ply moduli with constituent moduli (V_f = 0.6): (a) ply transverse modulus vs. fiber transverse modulus and matrix modulus; (b) ply shear modulus (in-plane or out-of-plane) vs. fiber shear modulus (in-plane or out-of-plane) and matrix shear modulus.

Besides the dependency between moduli shown above, the dependency of stress amplification factors **M** on constituent moduli, especially on E_m , also drew our attention. Since **M** varies over the entire cross-section of the unit cell model, plus it is a 6×6 matrix, it is neither possible nor necessary to investigate all **M**. Instead, we simply selected a number of points of interest where maximum stress concentration might occur under various loading conditions. Considering that the maximum longitudinal stress failure criterion was employed for fiber, among all 36 entries of an $\mathbf{M}_f$ at any point in the fiber, only those that contribute to σ_{f11} are significant; moreover, since fiber is much stiffer and stronger than matrix in its longitudinal direction, those entries of $\mathbf{M}_f$ are far less sensitive to the degradation of E_m . On the other hand, degradation of matrix modulus definitely affects $\mathbf{M}_m$, and consequently alters micro stress distribution in the matrix.

Fig. 4 shows variation of $\mathbf{M}_m$ versus E_m at three points near the fiber-matrix interface for IM7/8551-7 (V_f = 0.6), whose constituent (fiber and matrix) properties were listed in Table 1 and

Table 2. The locations of the three points were shown in Fig. 4(g). We obtained these data points through direct finite element analysis: keeping fiber properties unchanged, and reducing matrix Young's modulus gradually. Interestingly, by observing the trend of variation, we were able to tell that most of entries would have non-zero values when $E_m = 0$.

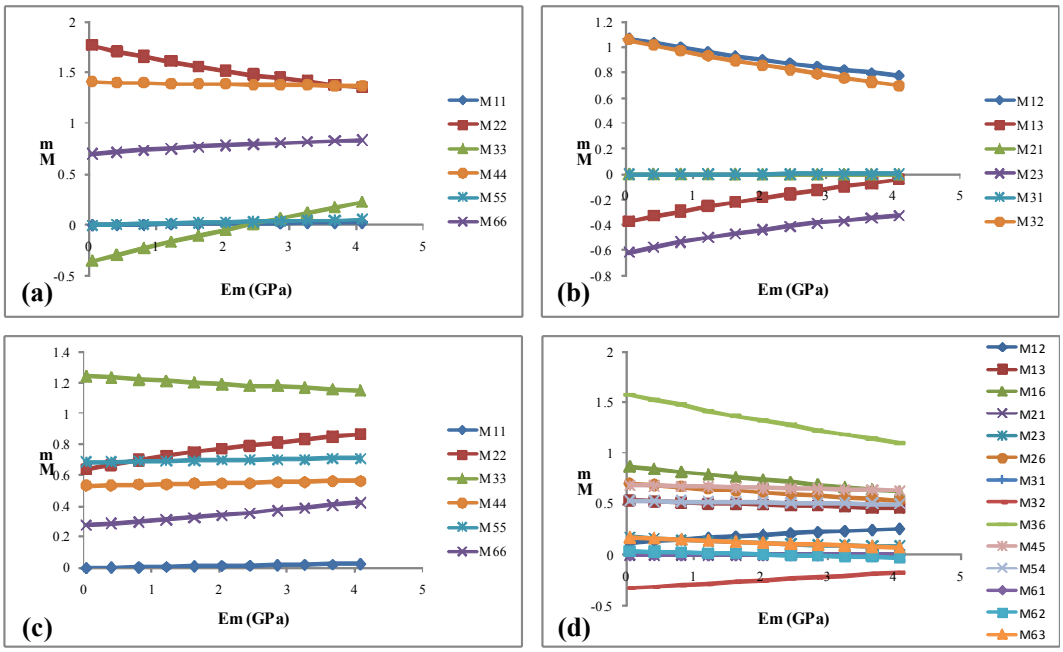

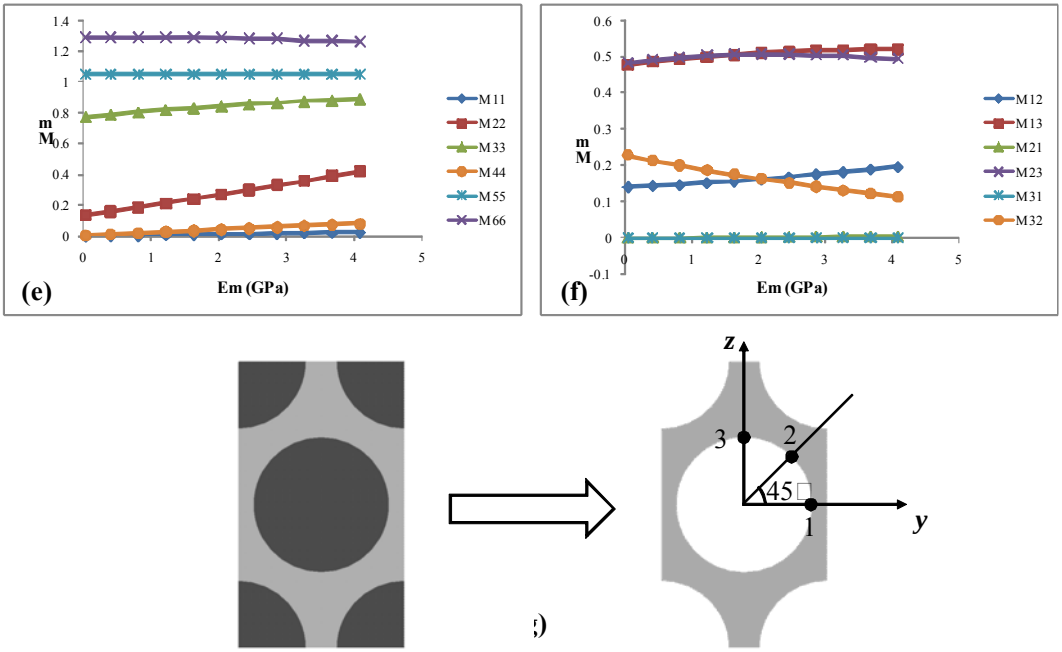

Fig. 4. Variation of $\mathbf{M}_m$ vs. E_m (IM7/8551-7, $V_f = 0.6$): (a) variation of diagonal entries of $\mathbf{M}_m$ at point 1; (b) variation of non-zero off-diagonal entries of $\mathbf{M}_m$ at point 1; (c) variation of diagonal entries of $\mathbf{M}_m$ at point 2; (d) variation of non-zero off-diagonal entries of $\mathbf{M}_m$ at point 2; (e) variation of diagonal entries of $\mathbf{M}_m$ at point 3; (f) variation of non-zero off-diagonal entries of $\mathbf{M}_m$ at point 3; (g) illustration of positions of point 1, 2, and 3.

FAILURE PREDICTION USING NONLINEAR MMF

We have run a number of cases to demonstrate the validity of this nonlinear MMF. The properties of various fibers and matrices we used for failure prediction were listed in

Table 1 and

Table 2, respectively.

Table 1. Mechanical properties of various fibers [8].

Fiber type	IM7	E-glass
Longitudinal modulus E_{f1} (GPa)	276	73
Transverse modulus E_{f2} (GPa)	13	73
In-plane shear modulus G_{f12} (GPa)	27	30.4
Major Poisson's ratio ν_{f12}	0.2	0.2
Major Poisson's ratio ν_{f13}	0.2	0.2
Transverse shear modulus G_{f23} (GPa)	7	45
Longitudinal tensile strength T_f (MPa)	4210	2150
Longitudinal compressive strength C_f (MPa)	2640	1450

Longitudinal thermal coefficient α_{f1} (10^{-6}/°C)	-0.4	4.9
Transverse thermal coefficient α_{f2} (10^{-6}/°C)	5.6	4.9
Through-thickness thermal coefficient α_{f3} (10^{-6}/°C)	5.6	4.9

Table 2. Mechanical properties of various matrices [8].

Matrix type	8551-7	MY750
Elastic Modulus E_m (GPa)	4.08	4.6
Elastic Poisson's ratio ν_m	0.38	0.38
Initial tensile strength T_{mi} (MPa)	70	60
Final tensile strength T_{mf} (MPa)	110	77
Initial compressive strength C_{mi} (MPa)	111	111
Final compressive strength C_{mf} (MPa)	175	142
Thermal expansion coefficient α_m (10^{-6}/°C)	46.7	58
Shape parameter γ	1.5	1.5

Failure Prediction for Uniaxial Loading

Fig. 5 shows the comparison between test results and MMF predictions of transverse compressive stress-strain curves for two UDs, E-glass/MY750 and IM7/8551-7, with V_f = 0.6. With given constituent properties, the nonlinear MMF not only predicted the effective stiffness of the ply, but also accurately caught the initial and final failure of the ply. The theoretical predictions and experimental data are well-matched [8].

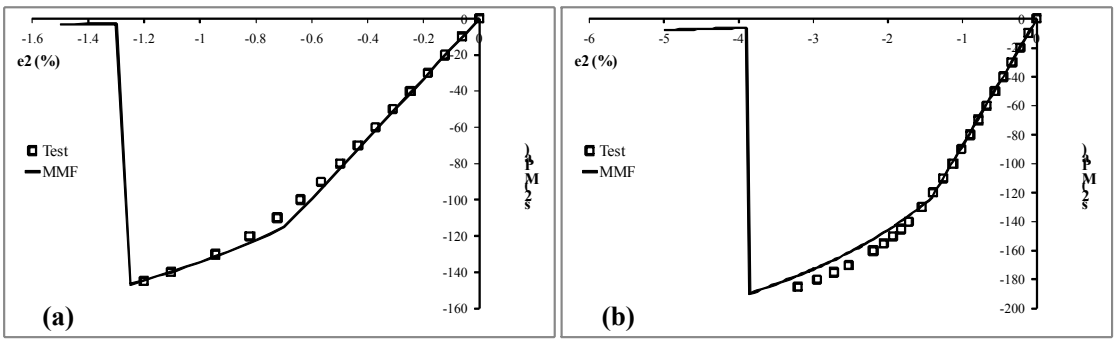

Fig. 5. Comparison between test results and MMF predictions of UD transverse compressive stress-strain curves: (a) E-glass/MY750; (b) IM7/8551-7.

Fig. 6 shows the uniaxial tensile stress-strain curves for IM7/8551-7 and E-glass/MY750 with two layup sequences: $[90/0]_{2S}$ and $[45/0/-45/90]_S$. The thickness of each ply and the fiber volume fraction were respectively set to be 0.125 mm and 0.6 in all cases, and a nominal strain of 5% was applied in all cases. Each curve features zigzag shape, resulting from constituent failure in plies. Fig. 6(a) is for IM7/8551-7 with stacking sequence of $[90/0]_{2S}$. Point A and B represent matrix final failure in 90° plies and fiber tensile failure in 0° plies, respectively. In Fig. 6(b), which is for IM7/8551-7 with layup sequence of $[45/0/-45/90]_S$, point C and D indicate matrix final failure in ±45° plies and fiber tensile failure in 0° plies, respectively; there is a considerable drop of stress right after

point D, and as the strain increases, the stress also increases based on a degraded stiffness until point E, denoting fiber compressive failure in 90° plies. For E-glass/MY750, however, fiber failure and matrix final failure are no longer as close as IM7/8551-7 cases. In Fig. 6(c), prior to point H, which indicates fiber tensile failure in 0° plies, we can observe matrix final failure in 90° plies and 0° plies, marked by point F and point G respectively. In Fig. 6(d), the situation is a little bit more complex: matrix final failure in 90° and ±45° plies occurs consecutively, indicated by point I and J; point K stands for matrix final failure in 0° plies, followed by point L, which means fiber tensile failure in 0° plies.

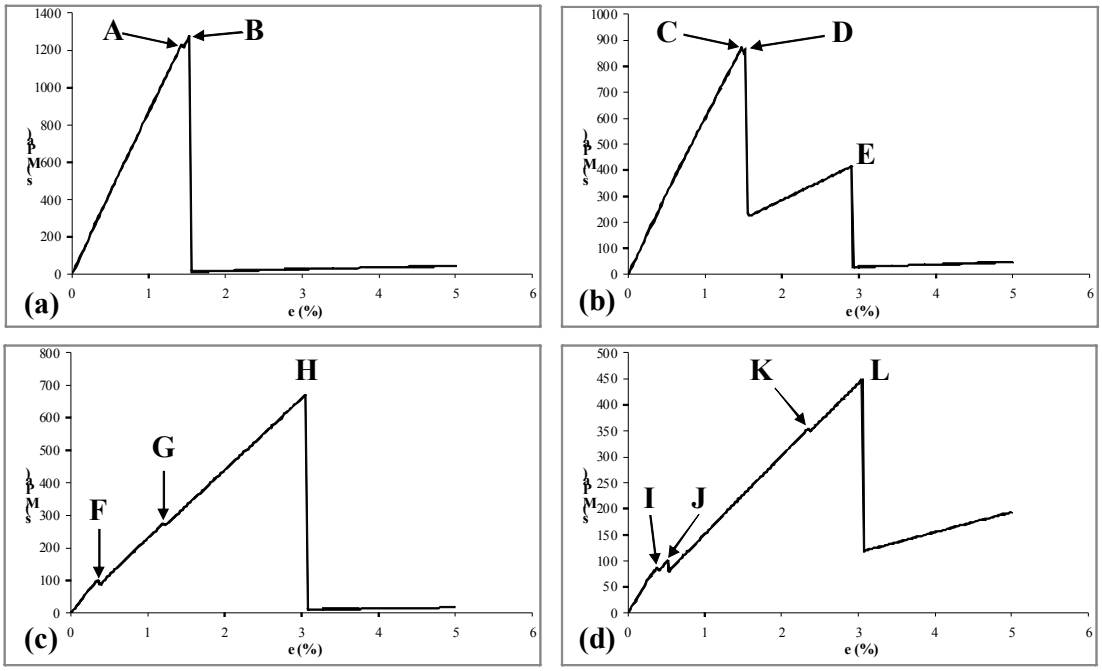

Fig. 6. Uniaxial tensile stress-strain curves of multi-directional laminates: (a) IM7/8551-7, $[90/0]_{2S}$; (b) IM7/8551-7, $[45/0/-45/90]_S$; (c) E-glass/MY750, $[90/0]_{2S}$; (d) E-glass/MY750, $[45/0/-45/90]_S$.

Fig. 7 shows the uniaxial compressive stress-strain curves for IM7/8551-7 and E-glass/MY750 with two layup sequences: $[90/0]_{2S}$ and $[45/0/-45/90]_S$. The thickness of each ply and the fiber volume fraction were respectively set to be 0.125 mm and 0.6 in all cases, and a nominal strain of 5% was applied in all cases. Each curve features zigzag shape, resulting from constituent failure in plies. The curve shown in Fig. 7(a) is for IM7/8551-7 with stacking sequence of $[90/0]_{2S}$. When the curve hits point A, fiber compressive failure occurs in 0° plies, therefore there is a great drop of stress value; however, 90° plies are still intact at this point, and as the strain keeps increasing, matrix initial failure occurs, resulting the nonlinear section of the curve from the drop after point A till point B, where matrix compressive failure occurs in 90° plies. In Fig. 7(b), we can see more peaks: point C is due to fiber compressive failure in 0° plies, whereas point D and E correspond to matrix and fiber compressive failure in ±45° plies respectively, and finally point F indicates matrix compressive failure in 90° plies. Although there are also two sharp points in Fig. 7(c), similar to Fig. 7(a), the physical reality represented by these two points is totally reversed: point G indicates matrix compressive failure in 90° plies while point H indicates fiber compressive failure in 0° plies. Before attaining point G, we can observe slight

nonlinearity due to matrix initial failure in 90° plies. In Fig. 7(d), point I, J, and K correspond to matrix compressive failure in 90° plies, matrix compressive failure in ±45° plies, and fiber compressive failure in 0° plies, respectively. For given strain (5%), fiber in ±45° plies remains intact, but if larger strain is provided, definitely there will be another peak after point K, showing fiber compressive failure in ±45° plies.

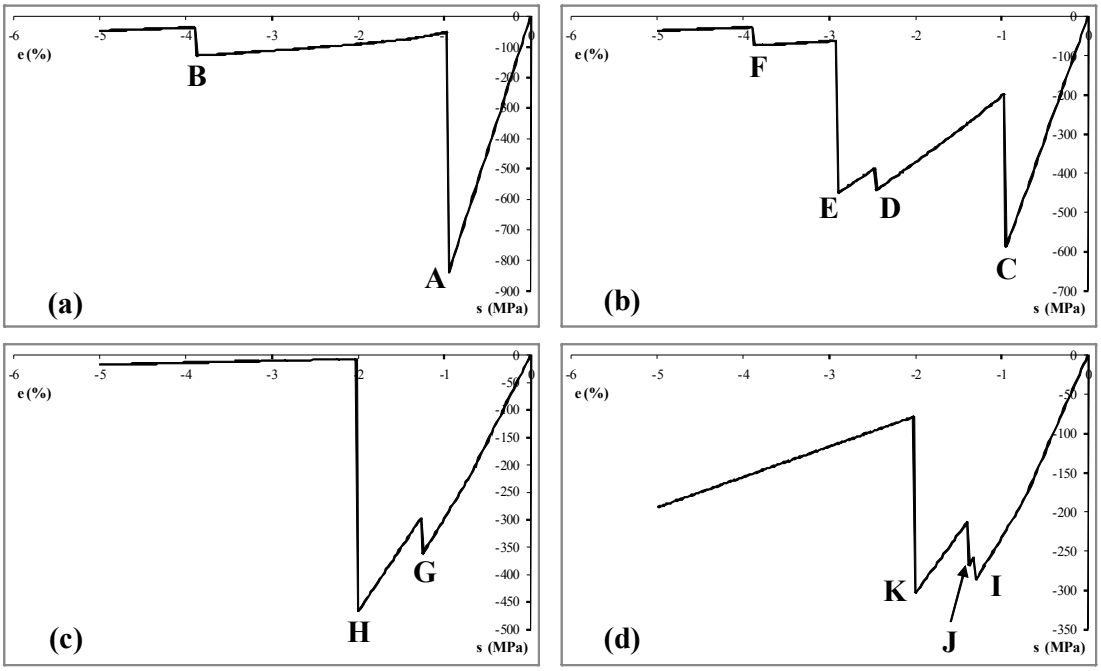

Fig. 7. Uniaxial compressive stress-strain curves of multi-directional laminates: (a) IM7/8551-7, $[90/0]_{2S}$; (b) IM7/8551-7, $[45/0/-45/90]_S$; (c) E-glass/MY750, $[90/0]_{2S}$; (d) E-glass/MY750, $[45/0/-45/90]_S$.

Failure Prediction for Multi-axial Loadings

Fig. 8 shows in-plane failure envelopes for IM7/8551-7 and E-glass/MY750 with two layup sequences: $[90/0]_{2S}$ and $[45/0/-45/90]_S$. The thickness of each ply and the fiber volume fraction were respectively set to be 0.125 mm and 0.6 in all cases. Initial failure envelopes were plotted in dashed lines while final failure envelopes were in solid lines. Due to the symmetry of layup sequences, all failure envelopes are symmetric about the line along which $\sigma_1 = \sigma_2$. Fig. 8(a) shows the initial and final failure envelopes of IM7/8551-7 with a stacking sequence of $[90/0]_{2S}$. Point A represents matrix final failure in all plies, and point G represents fiber tensile failure in all plies. Line segments AB and AF (both without endpoints) indicate matrix final failure in 0° and 90° plies respectively; whereas line segments GB and GF (both without endpoints) indicate fiber tensile failure in 90° and 0° plies respectively. At point B and F, the initial and final failure envelopes start to emerge as one, which means failure is dominated by fiber failure. This fact is also observable in Fig. 6(a), which corresponds to either point B or F: fiber fails right after matrix final failure. Sections BC and FE (both without endpoints) result from fiber tensile failure in 90° plies accompanied by matrix final failure in 0° plies, and fiber tensile failure in 0° plies accompanied by matrix final failure in 90° plies, respectively. Point C and E are turning points, at which fiber tensile/compressive failure occurs in all plies. To be more precise,

point C indicates the concurrence of fiber tensile failure in 90° plies and fiber compressive failure in 0° plies, while point E indicates the opposite case: fiber tensile failure in 0° plies and fiber compressive failure in 90° plies. Sections CD and ED (both without endpoints) are attributed to fiber compressive failure in 0° plies accompanied by matrix final failure in 90° plies, and fiber compressive failure in 90° plies accompanied by matrix final failure in 0° plies, respectively. At point D, fiber compressive failure occurs in all plies.

Fig. 8(b) gives the initial and final failure envelopes of IM7/8551-7 with layup sequence of $[45/0/-45/90]_S$. Point H, L, and J stand for matrix final failure in all plies, fiber tensile failure in all plies, and fiber compressive failure in all plies, respectively. Line segments HI and HK (both without endpoints) represent matrix final failure in 0° plies and 90° plies, respectively. The final failure envelope is ascribed to fiber failure in multiple plies: segments LI and LK (both without endpoints) are respectively owing to fiber tensile failure in ±45°, 90° plies and ±45°, 0° plies; while segments IJ and KJ (both without endpoints) are due to fiber failure in 0°, 90° plies (IJ & KJ, most of the second & fourth quadrants), fiber compressive failure in ±45°, 0° plies (IJ, the third quadrant), and fiber compressive failure in ±45°, 90° plies (KJ, the third quadrant).

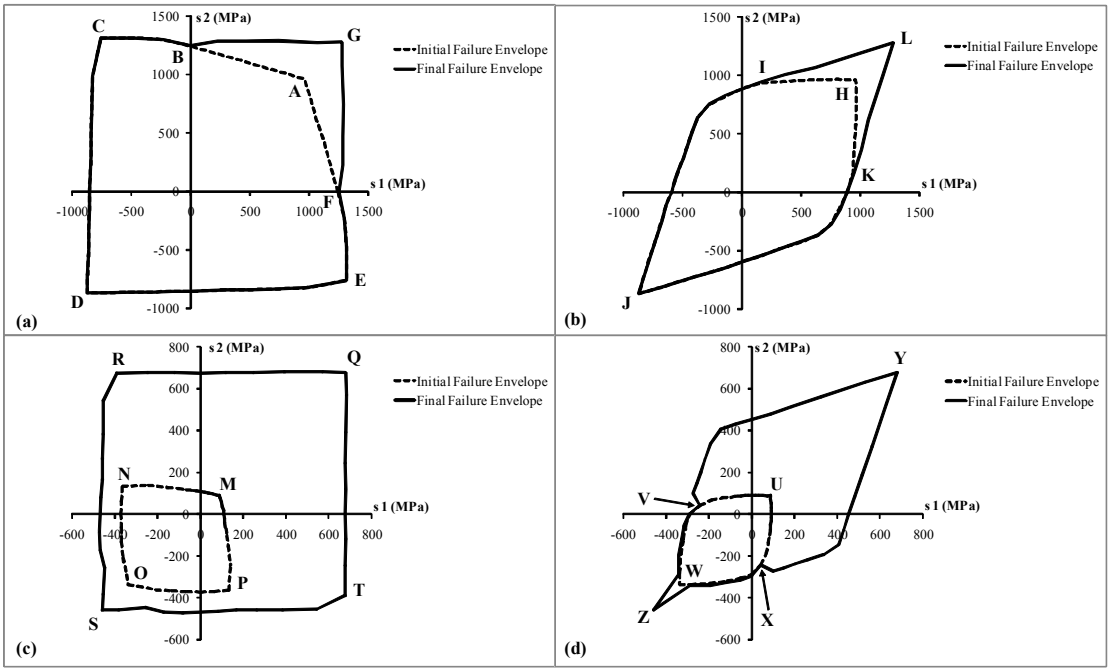

Fig. 8. In-plane failure envelopes of multi-directional laminates: (a) IM7/8551-7, $[90/0]_{2S}$; (b) IM7/8551-7, $[45/0/-45/90]_S$; (c) E-glass/MY750, $[90/0]_{2S}$; (d) E-glass/MY750, $[45/0/-45/90]_S$.

Fig. 8(c) shows initial and final failure envelopes of E-glass/MY750 with a layup sequence of $[90/0]_{2S}$. Referring to results shown in Fig. 6 and Fig. 7, we can conclude that under uniaxial tension/compression, for the given two different layup sequences, E-glass/MY750 always has matrix final failure prior to fiber failure. This conclusion also holds for Fig. 8(c). The initial failure envelope, which is due to matrix final failure, is completely separated from the final failure envelope, which is due to fiber failure. At point M and O, matrix in all plies fails; line segments MN and MP (both without endpoints) denote matrix final failure in 0° and 90° plies, respectively; on the contrary, line segments

NO and PO (both excluding point O) denote matrix final failure in 90° and 0° plies, respectively. Points Q and S correspond to fiber tensile and compressive failure in all plies; whereas fiber tensile failure in 90° plies concurs with fiber compressive failure in 0° plies at point R, and fiber tensile failure in 0° plies concurs with fiber compressive failure 90° plies at point T. Section QR, QT, RS, and TS (all without endpoints) corresponds to fiber tensile failure in 90° plies, fiber tensile failure in 0° plies, fiber compressive failure in 0° plies, and fiber compressive failure in 90° plies.

Fig. 8(d) illustrates the initial and final failure envelopes of E-glass/MY750 with layup sequence of $[45/0/-45/90]_S$. Point U, W represent matrix final failure in all plies, and point Y, Z respectively represent fiber tensile failure and compressive failure in all plies. Line segments UV and UX (both without endpoints) are attributed to matrix final failure in ±45°, 0° plies and ±45°, 90° plies, respectively; while matrix final failure in ±45°, 90° plies and ±45°, 0° plies contributes to the formation of segments VW and XW (both excluding point W), respectively. Considering the final failure envelope, segment YV and YX (both without endpoints) result from fiber tensile failure in ±45°, 90° plies (YV, the first quadrant), fiber tensile failure in ±45°, 0° plies (YX, the first quadrant), fiber tensile failure in 90° plies and fiber compressive failure in 0° plies (YV, the second quadrant), fiber tensile failure in 0° plies and fiber compressive failure in 90° plies (YX, the fourth quadrant). In the third quadrant, though the initial and final envelopes are quite close, they do not merge, meaning matrix final failure always precedes fiber failure. Sections VZ and XZ (both without endpoints) are mainly caused by fiber compressive failure in ±45°, 0° plies and ±45°, 90° plies, respectively.

CONCLUSION

With current MMF theory and the progressive damage model, we were able to predict the nonlinear mechanical behavior of UD and multi-directional laminate under various loading conditions, once the nonlinear behavior of matrix is known. In this paper we presented our prediction for several cases, which involve both UD and multi-directional laminates made of different fiber/matrix systems, and multi-axial loading conditions. The current MMF theory is based on linear elasticity, which could be less accurate and less realistic, but its full 3-D capability allowed us to obtain prediction results without any difficulty. We are keeping updating the MMF theory as well as the progressive damage model, in order to provide more accurate failure prediction with less effort.

ACKNOWLEDGEMENT

Authors thank the Stanford Composites Design Team headed by Prof. Stephen Tsai at Stanford University for technical discussion and collaboration. The development of the MMF has been partially funded by AFOSR with Dr. Charles Lee as a technical monitor.

References

1. Tsai SW. Strength & Life of Composites. JEC 2009.

2. Jin KK, Huang YC, Ha SK. Distribution of micro stresses and interfacial tractions in unidirectional composites. Journal of Composite Materials 2008; 42: 1825-1849.

3. Ha SK, Jin KK, Huang YC. Micromechanics of failure (MMF) for continuous fiber reinforced composites. Journal of Composite Materials 2008; 42: 1873-1895.

4. Raghava RS, Caddell RM, Yeh GSY. The macroscopic yield behavior of polymers. Journal of Material Science 1973; 8: 225-232.

5. Murakami S, Kamiya K. Constitutive and damage evolution equations of elastic-brittle materials based on irreversible thermodynamics. International Journal of Mechanical Sciences 1997; 39(4): 473–486.

6. MD Nastran R3 documentation

7. Abaqus version 6.7 documentation.

8. Kaddour AS, Hinton MJ. Instructions to contributors of the Second World-Wide Failure Exercise (WWFE-II): Part(A).

Previous Paper ***Back to Programme*** ***Back to Topic***